Original Article

SHM Structural Health Monitoring

Structural Health Monitoring
2016, Vol. 15(1) 50–64

DOI: 10.1177/1475921715623358
shm.sagepub.com
SAGE

Multi-damage localization on large complex structures through an extended delay-and-sum based method

Shengbo Shan[1], Jinhao Qiu[1], Chao Zhang[1], Hongli Ji[1] and Li Cheng[2]

Abstract

In this work, the technique of the delay-and-sum method has been extended to the localization of multi-damage on large complex structures. Through a case study by locating multiple damages on a composite aircraft panel, the exact extensions of the method are clearly presented. A multi-damage detection method is first designed on the basis of the propagating characteristics of Lamb waves as the preprocessing of damage localization. In light of the high signal complexity induced by the structural characteristics, an adaptive valid data extraction strategy is presented, improving the adaptability of the delay-and-sum method for complicated structures in terms of the damage localization accuracy. Since the localization accuracy of the delay-and-sum method can be significantly influenced by the uncertainty of preset velocity, it is further assessed by a quantitative localization accuracy evaluation method, revealing some fundamental features of the method in a comprehensive way. In addition, a boundary processing approach is designed to extend the delay-and-sum method for the multi-damage case. Experimental results in different damage situations verify that multi-damage can be located accurately by the proposed extended method.

Keywords

Lamb waves, multi-damage, delay-and-sum method, localization accuracy, complex structures

Introduction

Structural health monitoring (SHM), which characterizes various defect-related changes in structures in an online and real-time perspective, proves itself a promising tool to reduce the risks of structural failure.[1–3] Among various SHM tools, the Lamb wave–based method became the research highlight due to its appealing advantages like high sensitivity to damage and large monitoring range.[4–6] A Lamb wave–based SHM problem typically involves four main issues. The first is the fundamental mechanism which supports the damage monitoring methods, focusing on the propagating characteristics of Lamb waves.[7–10] Second, integrated monitoring system is essential to generate expected Lamb wave modes and capture the response signals. In the monitoring system, transducer plays an important role and there are many kinds of transducers covering different purposes. Some of them worth mentioning are angle beam transducers,[11] electromagnetic acoustic transducers,[12] laser sources,[13,14] and piezoelectric elements.[15,16] The third element is the signal processing approach which extracts expected damage information from the response signals, for example, amplitude, time of flight (ToF), and so on. Relevant approaches are mainly classified into three categories: time-series analysis, frequency analysis, and integrated time–frequency analysis.[17] The fourth element is the appropriate damage identification algorithm to determine the status of the monitoring structure.[17] It takes advantage of the extracted information and realizes damage identification.

Development on the damage localization methods is a significant area in the Lamb wave–based SHM field. Particularly, damage diagnostic imaging algorithms have been attracting increasing preference because they

[1]The State Key Laboratory of Mechanics and Control of Mechanical Structures, Nanjing University of Aeronautics and Astronautics, Nanjing, China
[2]Department of Mechanical Engineering, The Hong Kong Polytechnic University, Kowloon, Hong Kong

Corresponding author:
Jinhao Qiu, The State Key Laboratory of Mechanics and Control of Mechanical Structures, Nanjing University of Aeronautics and Astronautics, Nanjing 210016, China.
Email: qiu@nuaa.edu.cn

result in an interpretable and intuitive image to reflect the location of damage.[18] Some representative algorithms are phase arrays approach,[19] tomography technique,[20] probability-based diagnostic imaging (PDI) method,[21,22] and delay-and-sum algorithm.[23–26] For the tomography and PDI method, they use the limited spatial damage information provided by the actuator–sensor paths to reconstruct the damage image. As to the phased array method, it requires a number of transducers to perform as the actuator. Therefore, the localization accuracies of these methods are highly dependent on the density of transducers. In contrast, the most attractive factor of the delay-and-sum method lies in that it makes full use of the continuous time information and the preset velocity to reconstruct the continuous spatial damage information. Theoretically, only four transducers will make it to accurately locate damage anywhere in an infinite rectangular monitoring area. This property carries the method to our research interest. However, it has to be highlighted that damage localization accuracy of this method will be deteriorated by the uncertainty of preset velocity.

The delay-and-sum imaging algorithm was initially proposed by Wang et al.[23] to locate the bonded mass on an isotropic aluminum plate. CT Ng and M Veidt[24] modified the delay-and-sum algorithm using different group velocities in different directions to detect defects in composite flat plate. Z Sharif-Khodaei and MH Aliabadi[25] proposed a windowed energy arrival method (WEAM) to improve the delay-and-sum imaging method to locate damage on both a flat composite panel and a stiffened composite panel. They also sought to assess the delay-and-sum method by setting different velocities to the monitoring system. Nevertheless, the monitoring structure was small in size and their assessment process was just based on a single damage case in the experiment. The fundamental features of the method were not comprehensively revealed in their work.

When monitoring large complex structures, there are a few issues limiting the direct use of the delay-and-sum method. The propagating characteristics of Lamb waves in complex structures will be complicated, resulting in high signal complexity. Furthermore, the structure may suffer from multi-damage which may cause interference in terms of Lamb waves propagation.[26] Motivated by the above-addressed challenges, Qiu et al.[27] proposed a multi-damage monitoring method for a large-scale composite panel. They developed a damage index merging algorithm (DIMA) for damage detection and a weighted average multi-damage localization method based on the delay-and-sum imaging algorithm. However, the DIMA remains to be tested for structures where the geometric properties of monitoring subareas are not identical. In addition, the damage information in the resulted damage image is hard to be distinguished especially when damage locates on the boundary of adjacent subareas.

The major objective of this study is to extend the delay-and-sum method to achieve high localization accuracy for large complex structures under multi-damage cases. The article also attempts to provide better understanding of the properties of the method, which will further improve the adaptability of the method for engineering application.

The structure of the article is as follows. We first describe the experimental set-up as a study case for our methodology. Through the organization, the proposed methodology can be better presented. In section "Methodology," the exact extensions of the delay-and-sum methods are proposed. The multi-damage detection method is first designed as the preprocessing for the delay-and-sum method. A valid data extraction is developed to extend the method to achieve higher localization accuracy. We further evaluate the method to investigate its fundamental features. The boundary processing method is proposed to extend the method for the multi-damage case. Experimental tests are reported in section "Results" to prove the efficiency of the proposed methods. Finally, the article is concluded in section "Conclusion."

Experimental set-up

Composite aircraft panel and transducer network

As a study case, the structure of the carbon fiber–reinforced polymer (CFRP) aircraft panel is shown in Figure 1(a). The composite laminates consist of eight layers in a $[0°/90°/+45°/-45°]_s$ stacking sequence. There are several T-shaped stiffeners boned on the panel. Packaged piezoelectric wafer is selected as the transducer due to its advantages like fine dynamic characteristics, small size, low cost, and so on. Since the delay-and-sum method shows low dependence on the transducer density, the configuration of transducer array will be normally determined by the performance of the monitoring system and customer's requirement on localization error. In this study case, considering the attenuation property of Lamb waves in the CFRP panel and its geometric characteristics, the configuration of sensor network is designed. As shown in Figure 1(b), 16 piezoelectric wafers are attached to the panel covering a monitor dimension of 390×660 mm^2. The monitoring area is divided into nine subareas of equal size. Figure 1(c) illustrates the labels of the 16 sensors and the numbers of the nine subareas.

Automatic monitoring system

Figure 2 illustrates the experimental platform of the multi-damage localization system. The controller

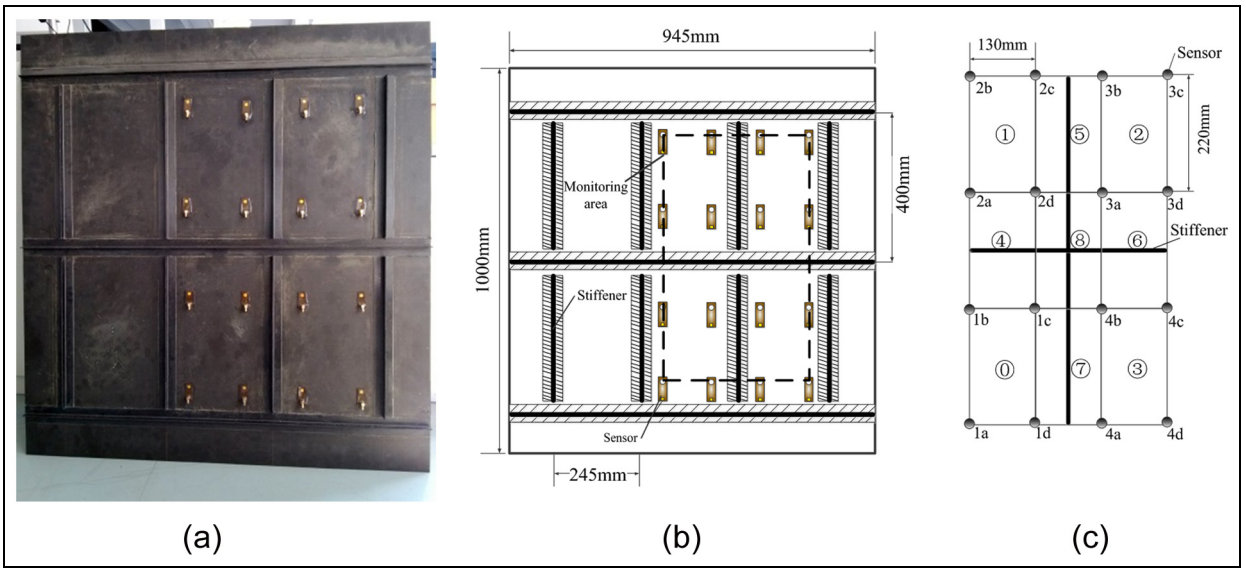

Figure 1. (a) CFRP aircraft panel and piezoelectric transducer arrangement, (b) schematic diagram of the panel, and (c) the division of the monitoring area.

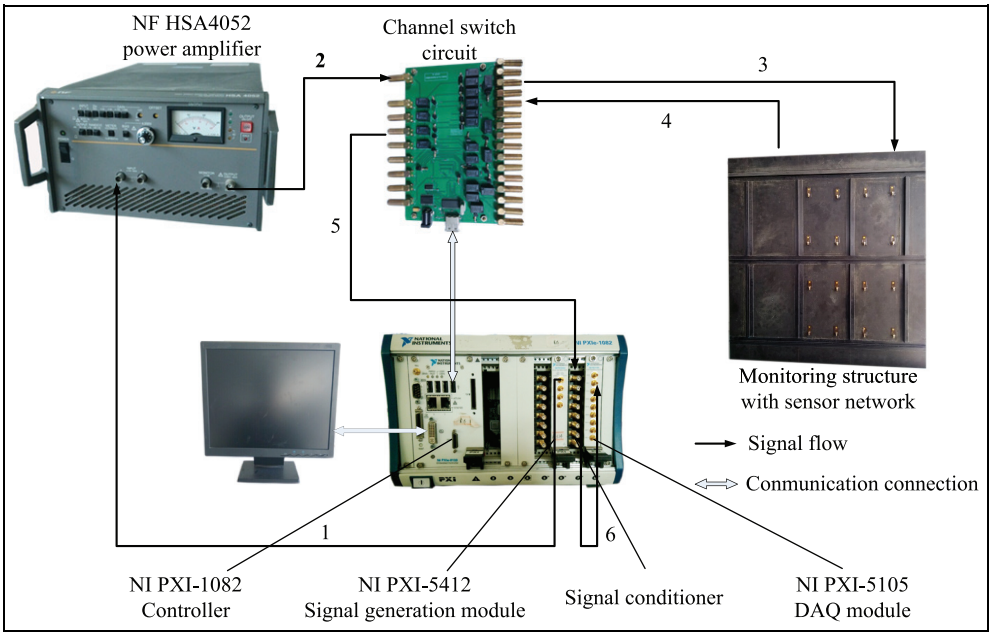

Figure 2. Experimental platform for the multi-damage monitoring system.

commands the NI-PXI5412 signal generating module to output an exciting signal. As the signal is amplified by the power amplifier and applied to the piezoelectric transducer, Lamb waves will be excited. The channel switch module is designed to ensure that each piezoelectric transducer works as an actuator in a certain order to improve the monitoring efficiency. Response signals of Lamb waves are processed in the signal conditioner and then acquired by the NI-PXI5105 data acquisition module. The signal conditioner is integrated with a charge amplifier and a band-pass filter. The controller finally stores and processes the data by our designed algorithms.

The selected exciting signal is a modulated five-cycle sine burst. It is a narrow-band signal which can be expressed as

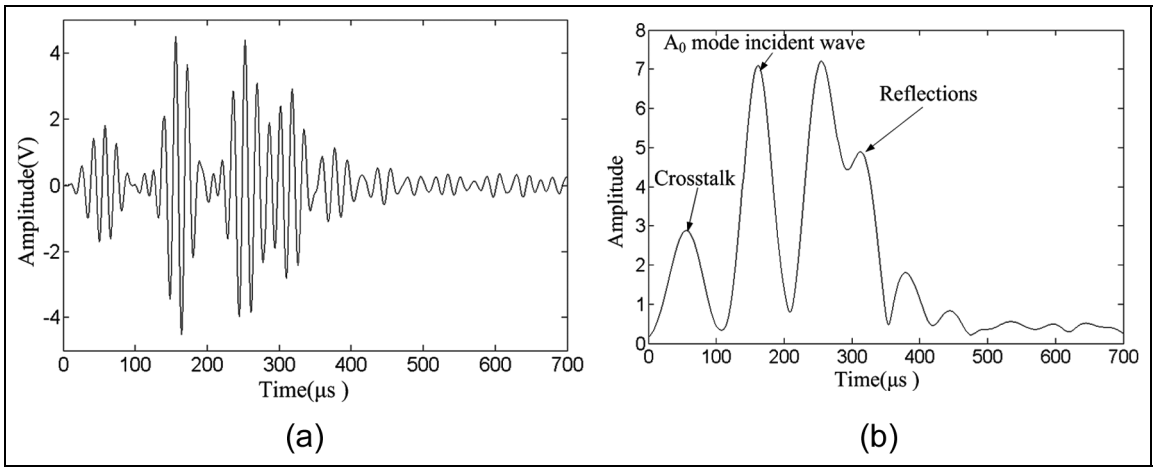

Figure 3. (a) Response signal captured by Sensor1b and (b) its complex Morlet wavelet coefficient modulus when Sensor1c performs as the actuator.

$$f_a(t) = A\sin(2\pi f_c t)\left(1 - \cos\left(\frac{2\pi f_c t}{5}\right)\right) \quad (1)$$

where A denotes the amplitude and f_c represents the central frequency of the signal (60 kHz in this study). At this frequency, the amplitude of A_0 mode Lamb waves is dominant in the response signals, which is preferred from the SHM viewpoint. The exciting signal with the amplitude of 1 V is amplified by the power amplifier to 60 V. The data acquisition module samples at 1 MHz for each channel. The response signals are amplified (100 times) and band-pass filtered (500 Hz–200 kHz) by the signal conditioner. Artificial damages are introduced in this study with a kind of solid adhesive tape. Just as the effect of actual damage, the geometry continuum can be interrupted by the solid tape.

Group velocity measurement

To obtain the velocities of Lamb waves, it requires the precise measurement of ToF. Complex Morlet transform is applied to the response signals to extract their envelopes.[28] The coefficient of the wavelet transform is expressed as

$$CWT_f(a,b) = \frac{1}{\sqrt{a}}\int_{-\infty}^{+\infty} f(t)\psi^*\left(\frac{t-b}{a}\right)\mathrm{d}t \quad (2)$$

$$\psi(t) = \frac{1}{\sqrt{\pi\gamma}}e^{j\omega_0 t}e^{-t^2/\gamma} \quad (3)$$

where a and b are the scale and translation factors. $\psi^*(t)$ represents the conjunction of $\psi(t)$ which is the complex Morlet wavelet mother function. ω_0 denotes the angular central frequency and γ is the width of Gaussian window. In this study, only the modulus of wavelet coefficient with a fixed scale factor is concerned which is related to the central frequency of the exciting signal. As the complex Morlet wavelet is a narrow-band signal, this process can diminish the influence of noise to a certain extent. Specifically, when Sensor1c performs as the actuator, the response signal of Sensor1b is acquired and its complex wavelet modulus is shown in Figure 3.

The measurement of velocities of Lamb waves is performed in Subarea0. Each transducer works as the actuator and the rest perform as the sensor in a certain order. The ToFs of A_0 mode Lamb waves can be obtained to calculate the corresponding group velocities which are shown in Table 1. In the monitoring system, a 1-μs error in the ToF may lead to more than 10-m/s error in the calculated velocity. In this light, it is assumed that there is no significant difference within the measured velocities in different directions. Finally, the average of the calculated velocities is regarded as the group velocity of Lamb wave in the CFRP structure, in this case 1139 m/s.

Methodology

As damage is usually considered as the scattering source in a typical Lamb wave–based SHM method, the most important task is to capture the damage-induced scattering signals accurately.[29,30] Normally, it is hard to interpret the response signals in a complex monitoring structure so that baseline signals are required to be first registered in the intact condition. In the monitoring process, the corresponding response signals (measured signals) will be compared with the baseline signals. Specifically, residual signal is defined by measured signals subtracted by baseline signals, as

Table 1. Measurement of group velocity of Lamb waves in the CFRP panel.

Actuator	Sensor			
	1a	1b	1c	1d
1a	-	1193 m/s	1126 m/s	1087 m/s
1b	1206 m/s	-	1136 m/s	1192 m/s
1c	1146 m/s	1136 m/s	-	1077 m/s
1d	1055 m/s	1100 m/s	1190 m/s	-

CFRP: carbon fiber–reinforced polymer.

$$R(t) = D(t) - H(t) \tag{4}$$

where $D(t)$ and $H(t)$ are the measured response signal and baseline signal, respectively.

Multi-damage detection based on the Lamb wave propagating characteristics

As part of the task of damage localization, detection of multi-damage existence on the monitoring structure needs to be first addressed. Two parameters are defined which are closely related to the health status of the structure. The first parameter named damage index of actuator–sensor path (*DIASP*) reveals the difference between measured response signal and baseline signal of one specific actuator–sensor path. The second parameter is called damage index of area (*DIA*) which denotes the possibility of damage existence in the subarea. *DIASP* and *DIA* can be expressed as

$$DIASP = \int_{2t_{\text{off}}}^{t_{\max}} \text{abs}(CWT_{R(t)}(a,b))\text{d}b \tag{5}$$

$$DIA(i) = \sum_{\Omega} DIASP \tag{6}$$

where t_{off} is the time offset caused by the Lamb wave exciting process and it is approximately equal to half of the length of the exciting signal. $t_{\max}$ is the maximum length of response signals which will be discussed in the valid data extraction section. Ω indicates that $DIA(i)$ of the ith subarea is obtained by adding up *DIASP* of some specific actuator–sensor paths in the area. Ω is closely related to the geometric property of the structure and the propagation characteristics of Lamb waves.

In this study case, the influence of damage on the propagating characteristics is analyzed in an experimental perspective. Two typical damage cases are highlighted, as shown in Figure 4. When damage is located in Subarea0 and Sensor1a is used as an actuator, the residual signal of Sensor1c has much larger amplitude than those of the other two sensors (Figure 4(a)). It indicates that a defect would cause the most significant signal change in the direct wave propagating path in a flat plate. Figure 4(b) illustrates the response residual signals of the sensors in Subarea7 when exciting signal is applied on Sensor1c. However, the residual signal of Sensor1d has the largest amplitude instead of that of Sensor4b on the actuator-damage path. In this case, as damage is considered as the scattering source, the damage-induced scattering Lamb waves will be reflected by the stiffener. The signal change in the direct wave path will become less significant. According to the characteristics, a multi-damage detection method can be designed for this study case.

Two different strategies for choosing proper Ω are applied to calculate the of *DIA* of all the subareas, as is

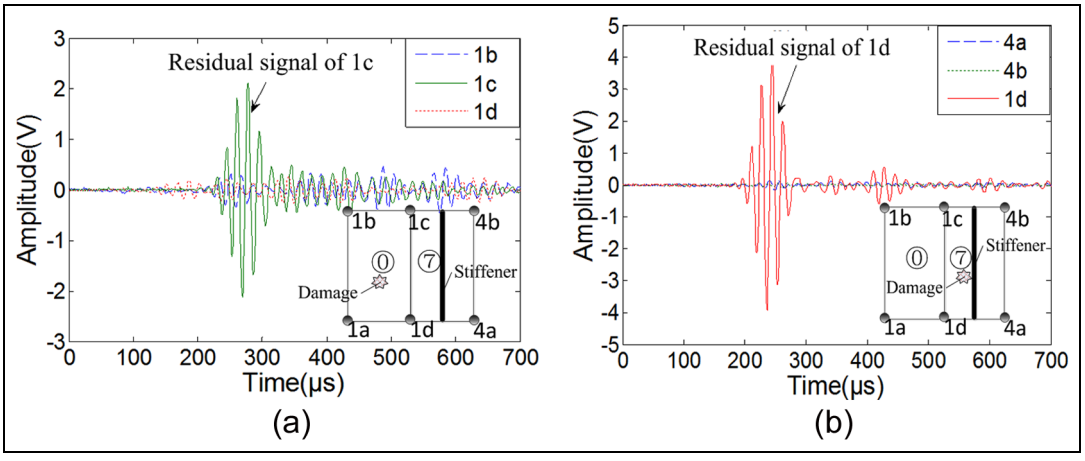

Figure 4. (a) Residual signals of Sensor1b, Sensor1c, and Sensor1d when Sensor1a performs as the actuator with damage locating in Subarea0, and (b) residual signals of Sensor4a, Sensor4b, and Sensor1d when Sensor1c performs as the actuator with damage locating in Subarea7.

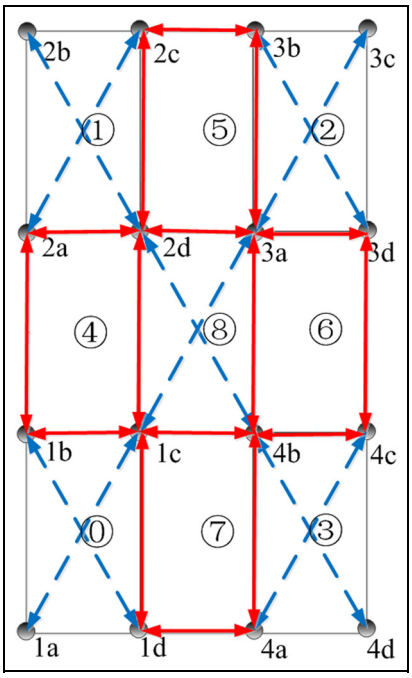

Figure 5. Actuator–sensor path choice strategy when calculating *DIA* of each subarea.

shown in Figure 5. In Subarea0, Subarea1, Subarea2, Subarea3, and Subarea8, *DIA* is obtained by adding up the *DIASP* of diagonal actuator–sensor paths (the dashed lines with arrows). However, the *DIA* of Subarea4, Subarea5, Subarea6, and Subarea7 is calculated by adding up the *DIASP* of actuator–sensor paths in the edge of the rectangular subarea (the solid lines with arrows).

The proposed multi-damage detection method has two advantages. First, this method chooses the actuator–sensor paths which are relatively most sensitive to damage in the subarea according to the propagating characteristics. It is effective to detect the occurrence of damage in each subarea. Second, interference between adjacent subareas is minimized which is of great benefit on multi-damage detection. For example, as shown in Figure 4(b), the *DIASP* of actuator–sensor path 1c–1d is much larger than that of other actuator–sensor paths. This value will only be added to the *DIA* of Subarea7 despite the fact that the actuator–sensor path 1c–1d belongs to Subarea0 too.

Delay-and-sum imaging algorithm for damage localization

The algorithm uses residual signals which are delayed and summed to obtain the damage possibility of each spatial point in the structure. The algorithm can be divided into four steps.

The first step is to calculate the expected arrival time of every point for all actuator–sensor paths. For a point in the structure, the arrival time of a signal traveling from actuator i at (x_i, y_i) to the point at (x, y) and on to sensor j at (x_j, y_j) can be calculated as

$$t_{ij}(x,y) = t_{\text{off}} + \frac{\sqrt{(x-x_i)^2+(y-y_i)^2} + \sqrt{(x-x_j)^2+(y-y_j)^2}}{v} \tag{7}$$

where v is the group velocity of Lamb waves.

As different actuator–sensor paths have different sensitivity to damage, the second step is to normalize the residual signals. The necessity is proved by the huge difference in the amplitude of residual signals of different actuator–sensor paths in Figure 4. The normalization process ensures that all actuator–sensor paths provide sufficient damage information in the damage imaging process. It can be expressed as

$$\overline{R(t)} = \frac{R(t)}{\max\left(\text{abs}(R(t))\right)} \tag{8}$$

The third step is to calculate the complex Morlet wavelet coefficient modulus of the residual signals to extract damage information for further imaging process. It is performed as

$$E(b) = \text{abs}(CWT_{\overline{R(t)}}(a,b)) \tag{9}$$

The final step is to calculate the damage possibility of every point and obtain the damage image of the monitoring area. Each residual signal is delayed by the calculated time $t_{ij}(x, y)$. The corresponding damage image of a specific actuator–sensor path is a set of ellipses. Signals from all actuator–sensor paths are summed to obtain the damage possibility of each spatial point. In the damage image, the possibility is set to be the pixel value, as

$$P(x,y) = \sum_{i=1}^{N-1} \sum_{j=i+1}^{N} E(t_{ij}(x,y)) \tag{10}$$

where N is the number of transducers in the monitoring area. It can be concluded that damage will be highlighted in the damage image with the highest pixel value.

Adaptive valid data extraction

When Lamb waves run into stiffeners or the boundaries, they will be reflected. Residual signal usually contains the damage-induced scattering part and the

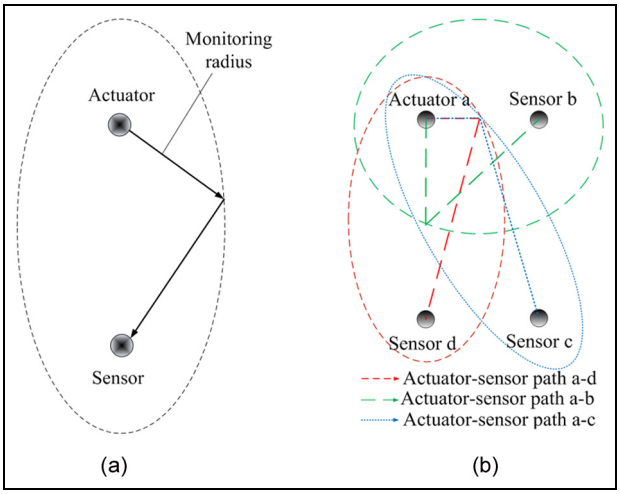

Figure 6. (a) Sketch of monitoring radius and (b) the designing strategy of the monitoring radius.

boundary reflecting part and the undesired reflecting part in the residual signals will deteriorate the localization accuracy. In addition, when damage is distant to the actuator–sensor path, the amplitude of the residual signals will be attenuated. In this case, damage-induced scattering signals may be inevitably polluted by noises.

With careful consideration of the length of response signals, there may be solutions to the problems. In this study, the concept of monitoring radius of actuator–sensor path is introduced. It is defined as the length of the long axis of the ellipse within which the actuator–sensor path can provide effective damage information, as shown in Figure 6(a). When damage locates outside the monitoring radius of a specific actuator–sensor path, we believe the damage information provided by the path is inaccurate and it will be ignored in the designed monitoring methods. Essentially, determination of the monitoring radius is identical to consideration for the signal length. In this article, a two-step adaptive valid data extraction strategy is proposed.

Step 1. The first step is to design the appropriate monitoring radius. Figure 6(b) illustrates the designing strategy for monitoring radius for a rectangular sensor array. The ellipse corresponding to the monitoring radius passes through the midpoint of the other edge of the rectangular monitoring area. This strategy ensures that for each point in the subarea, at least three actuator–sensor paths can provide damage information. Meanwhile, the influence of reflection of Lamb wave is diminished to a fairly large extent. The maximum length of response signals is estimated as

$$t_{\max} = \frac{r_{\mathrm{mr}}}{v} + 2t_{\mathrm{off}} \tag{11}$$

where r_{mr} denotes the monitoring radius.

Step 2. When damage is close to the actuator–sensor path, there may still be reflection parts in the response signals after the first process. The second step is proposed in this condition, but it is only for the damage localization process. Due to the short distance between the damage and the actuator–sensor path, the damage-induced scattering wave packet can be easily separated from the residual signal and it is the first arrival. These signals will be truncated again to obtain the optimal length for damage localization. The optimal length of the response signals is expressed as

$$t_{\mathrm{optimal}} = \begin{cases} t_{\mathrm{fa}} + t_{\mathrm{off}} & \left(t_{\mathrm{fa}} < \frac{r_{\mathrm{mr}}}{v} + t_{\mathrm{off}}\right) \\ t_{\max} & (\text{otherwise}) \end{cases} \tag{12}$$

where t_{fa} denotes the time of the first arrival.

Evaluation of localization accuracy

When locating damage with the delay-and-sum algorithm, the parameters set to the system are the group velocity of Lamb waves and the coordinates of the transducers. In practical application, the coordinates of the transducers can be precisely obtained while it is almost impossible to match the preset velocity and the actual velocity. In the following section, the extent of the localization accuracy deterioration caused by the deviation of the preset velocity is researched. Four steps are designed in the evaluation process:

Step 1. It is assumed that the actual damage locates at a certain point (x, y) in the monitoring area. The normalized residual signals can be ideally reconstructed by shifting the exciting signal according to the geometric characteristics of the monitoring area and the actual group velocity.

Step 2. A deviation p of the actual velocity is considered and the resulting velocity v_{s} is set to the monitoring system

$$v_{\mathrm{s}} = v(1+p) \tag{13}$$

Step 3. The delay-and-sum algorithm is carried out to obtain the corresponding damage image with the reconstructed residual signals. In the damage image, the calculated damage position is usually regarded as the point where the pixel value reaches the maximum. The distance between the assumed actual damage position (x, y) and the calculated damage position $(x_{\mathrm{calculated}}, y_{\mathrm{calculated}})$ is defined as the localization error.

Step 4. The process is conducted to every point in the monitoring area, resulting in the localization error distribution $LED(x, y|p)$ for a given velocity deviation

$$LED(x, y|p) = \sqrt{(x - x_{\text{calculated}})^2 + (y - y_{\text{calculated}})^2} \quad (14)$$

Boundary processing

For large-scale structures, the monitoring area should usually be divided into a few subareas. When damage images of all subareas are obtained, all the images need to be put together according to their corresponding positions, outputting the damage image of the whole monitoring area. However, if damage locates on the boundary of adjacent subareas, it may be diagnosed in both the subareas and damage information will be redundant after synthesizing the damage images of all subareas. Under this circumstance, a boundary processing procedure is proposed to improve the multi-damage localization method.

After obtaining the damage images of all subareas, the boundary processing procedure starts. The distance between damages in adjacent subareas is calculated and compared with the preset threshold which is selected based on the results of localization accuracy evaluation. If the calculated distance is less than the threshold, it is considered that the damage images of adjacent subareas are resulted from a single damage on the boundary. The damage information of one subarea is wiped out according to the corresponding *DIA* of the monitoring subareas.

Multi-damage localization process

The whole multi-damage localization process for large complex structures is shown in Figure 7. After dividing the large monitoring area into a few subareas, damage detection procedure is carried out to obtain the numbers of the subareas with damages. The damage imaging algorithm is then applied to each damaged subarea separately. Eventually, the system outputs the damage image of the whole monitoring area by synthesizing

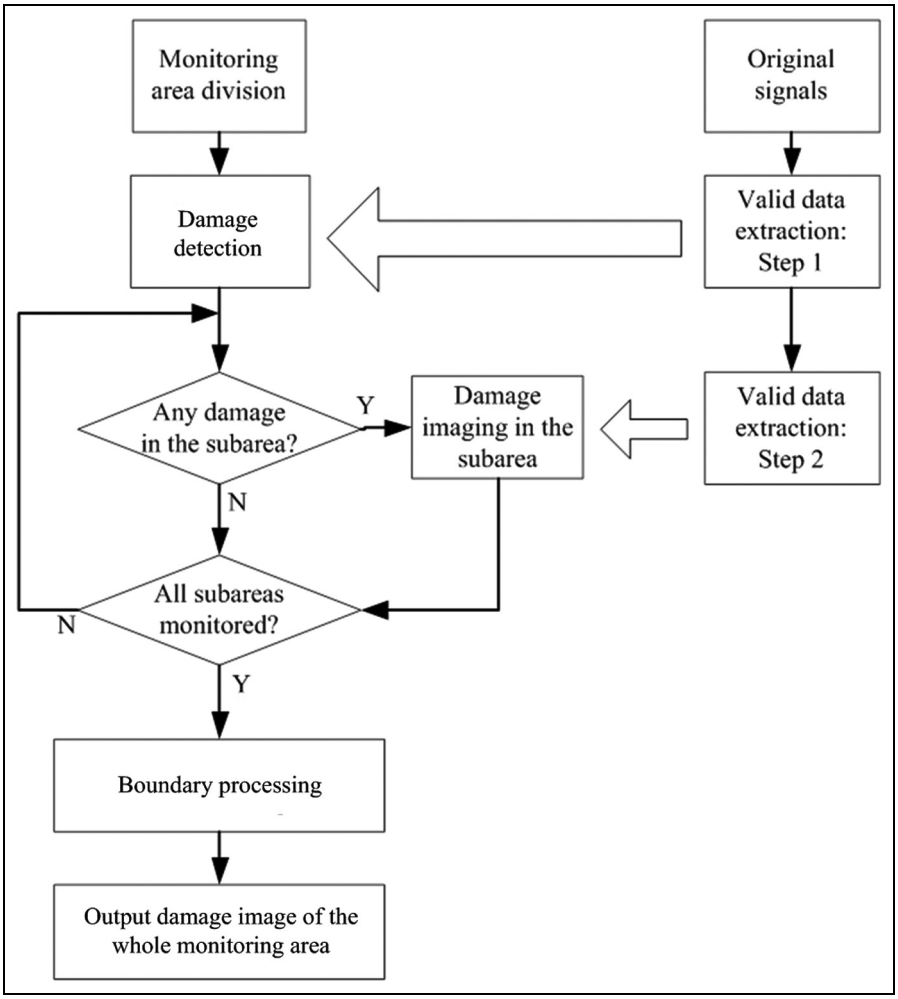

Figure 7. Process of the multi-damage localization method.

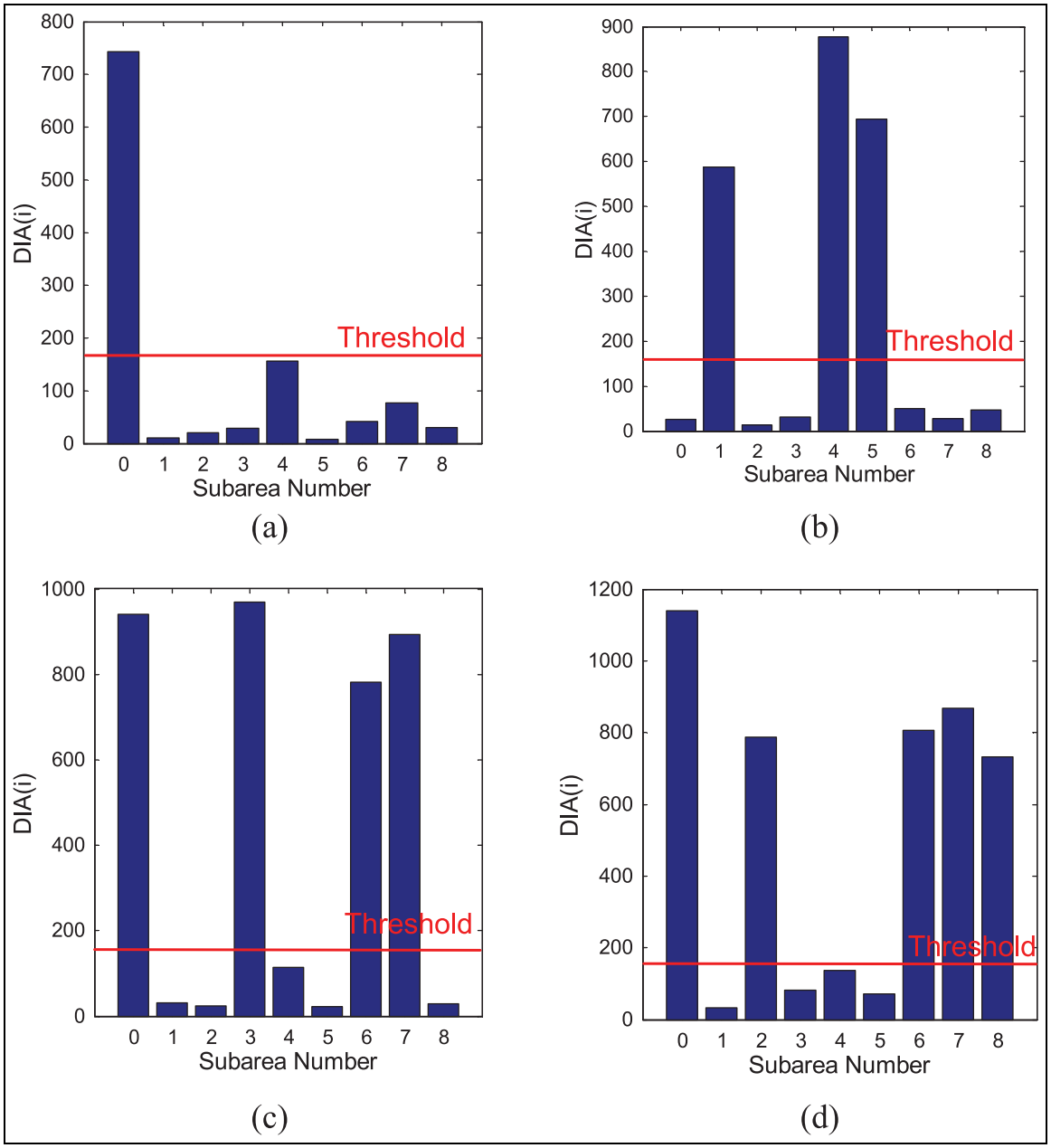

Figure 8. Multi-damage detection results when damages locate in Subarea: (a) 0; (b) 1, 4, and 5; (c) 0, 3, 6, and 7; and (d) 0, 2, 6, 7, and 8.

images of all the subareas with the boundary processing method.

Results

Multi-damage detection

In the experiments, solid tapes of 8 mm × 8 mm × 2 mm are stuck to the panel to simulate multi-damage. Four damage situations are considered and the results of damage detection are shown in Figure 8. Theoretically, each subarea needs a threshold to identify the occurrence of damage because the property of each transducer varies and different actuator–sensor paths are selected in different subareas. However, since the gap between the value of *DIA* in damaged subarea and undamaged subarea is huge, a single threshold is set to all subareas. During the experiments, the baseline signals are measured a few times and the corresponding *DIA* which is related to measurement noises is calculated. Results show that none of the calculated *DIA* exceeds 160 μ(V s), and this value is set to be the

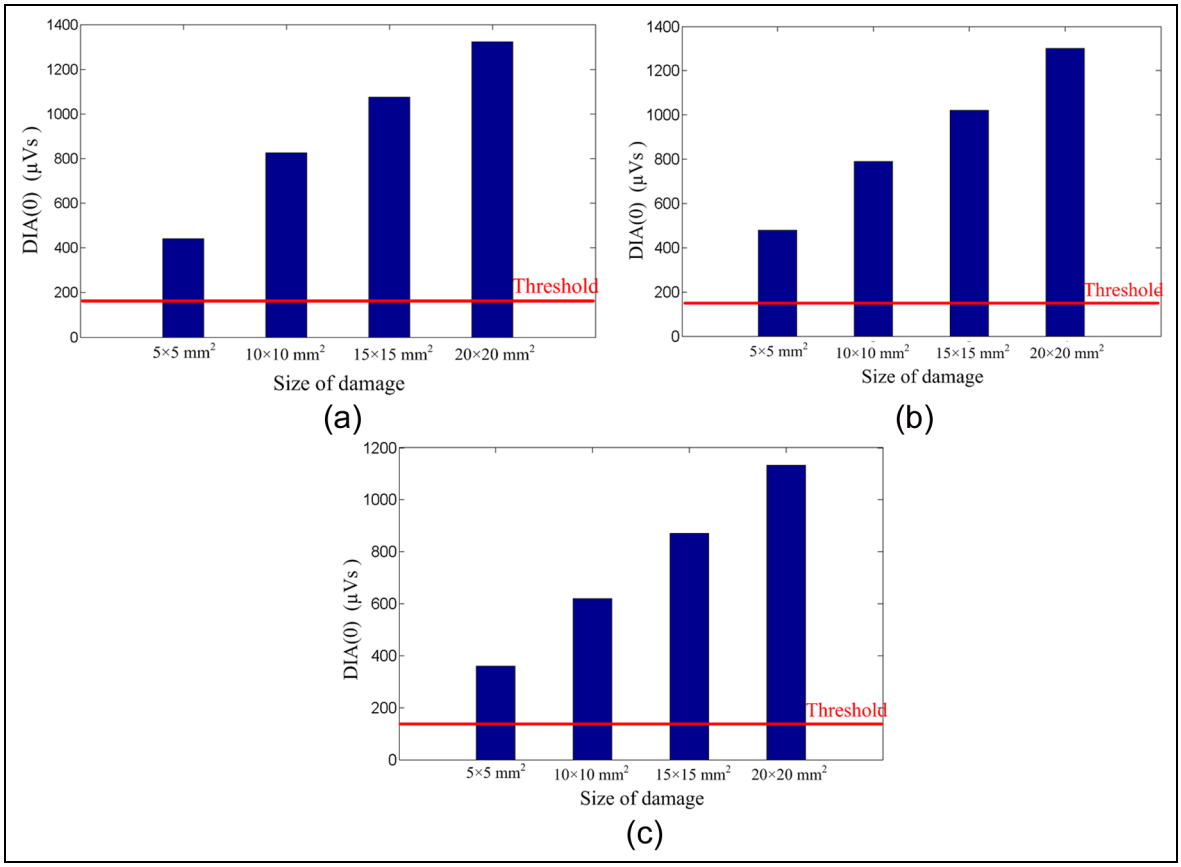

Figure 9. Sensitivity evaluation of the multi-damage detection method for Subarea (a) 0, (b) 7, and (c) 8.

threshold for the detection system. Results clearly prove the efficiency of the proposed multi-damage detection method.

The sensitivity of the multi-damage detection method is also preliminarily testified. The 2-mm-thick solid tapes of four different sizes are located in the center of three typical square subareas, Subarea0, Subarea7, and Subarea8, respectively. Results are shown in Figure 9. As the size of damage increases, the corresponding *DIA* increases. Damages can still be clearly detected when the size is as small as 5 mm × 5 mm. However, the sensitivity of the method requires to be further studied as the *DIA* does not only rely on the size of damages, but also their locations. To improve the ability of detecting smaller damages, a potential way is to increase the exciting frequency of Lamb waves. The issue will be investigated in our future works.

Damage localization with the valid data extraction

When locating damage in complex structures, a conventional approach to exact damage-induced scattering wave is to find the first arrival in the residual signal.[27] However, when damage is distant to the actuator–sensor path, the damage-induced scattering signal is more likely to be polluted by boundary reflection and noises. In this case, the false damage information will still be brought into the damage image.

In this research, the delay-and-sum imaging algorithm is applied with the valid data extraction strategy. To evaluate the proposed method, we place the artificial damage in Subarea0 and corresponding damage images are obtained in three different cases, which are shown in Figure 10. A nonlinear normalization is performed to stand out the high pixel value in the damage image.[27] Figure 10(a) shows the damage image which is obtained using the original residual signals directly. The localization accuracy is dramatically deteriorated by the reflection of Lamb waves. Damage image in Figure 10(b) is obtained using the conventional method. As predicted, the false information still has a disastrous effect on the localization accuracy. Figure 10(c) illustrates the damage image which is obtained with valid data extraction. It can be seen that the localization accuracy is significantly improved by the proposed strategy.

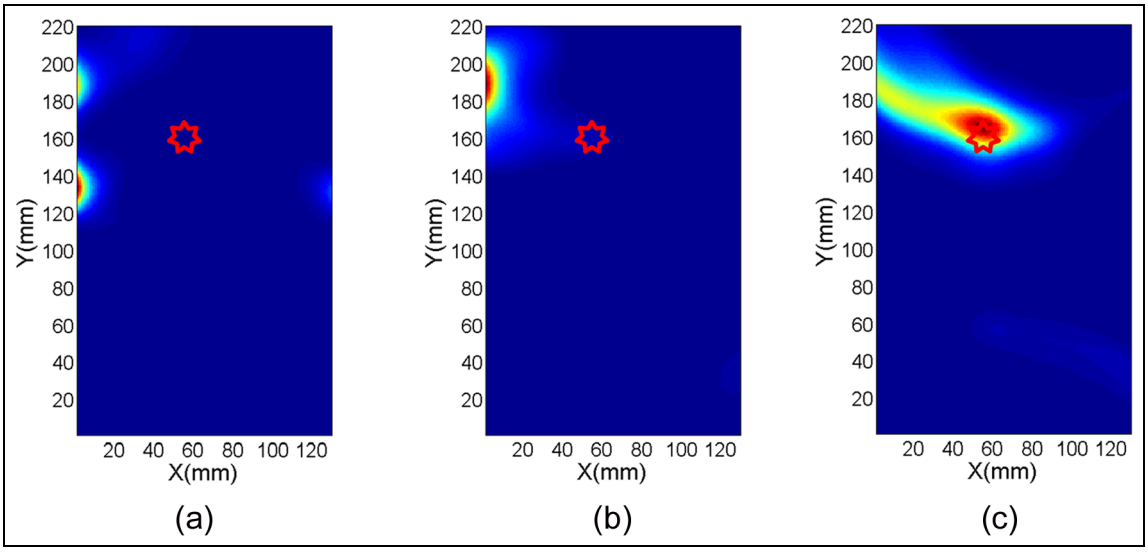

Figure 10. Calculated damage image using (a) residual signals directly, (b) residual signals processed by the conventional approach, and (c) residual signals processed by adaptive valid data extraction. (The star symbols represent the actual location of artificial damage.)

Figure 11 gives the illustration of multi-damage localization images of the different damage situations mentioned in the multi-damage detection section. All damages can be accurately located by the proposed method. However, unlike the multi-damage detection process, the damage imaging algorithm uses signals of all actuator–sensor paths in the subarea. As adjacent subareas share common sensor pairs, the localization accuracy in one subarea may be interfered by its adjacent subareas. The influence of the interference is hard to eliminate and it is the main cause of the localization error.

Evaluation of localization accuracy

According to the evaluation of localization accuracy process, some typical deviations of the velocity are set to the system and the corresponding localization error distributions are calculated and shown in Figure 12. From the results, a number of features of the imaging algorithm can be highlighted:

1. The localization error of a point in the monitoring area is closely related to the position of the point. If damage locates in the center of the monitoring area, the localization error is less sensitive to preset velocity deviation. In other words, central damages can be located more accurately.
2. When the deviation is getting larger, the absolute value of the localization error tends to become larger. However, the localization error distribution of the monitoring area hardly changes.
3. There is some difference between the localization error distributions in the positive and negative deviation situations. Specially, when damage locates near the edges of the monitoring area, huge sensitivity difference between the two situations can be observed.
4. The maximum value of the localization error is about 25 mm when the preset velocity variation is up to 8%. Since the calculated damage covers a certain area in the image and the damage itself has a fixed size, the localization error is acceptable in engineering applications. As a result, it can be concluded that the damage image method shows the great ability of robustness to the preset velocity variation.
5. When the deviation of velocity is within the range of $\pm 5\%$, which is approximately equal to the measured velocity deviation in this study, the maximum value of localization error is about 15 mm. The double of this value is selected as the threshold for boundary processing.

The localization error caused by preset velocity variation is also investigated in the experiment. Artificial damage is placed on the area where localization error is relatively more sensitive to the velocity variation. Figure 13 gives the illustration of the damage images of Subarea0 obtained by setting different velocities to the monitoring system. In this case, the measured average velocity (1139 m/s) is considered as the actual group velocity of Lamb wave in the structure for all directions. The deviations are based on this average value. As mentioned before, the deviation of velocity in the

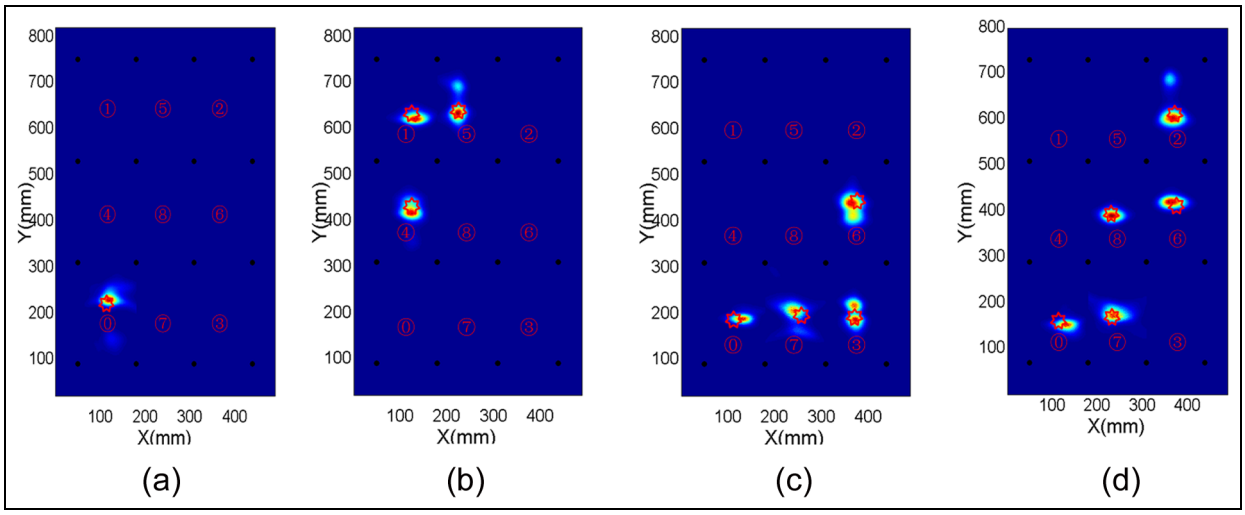

Figure 11. Damage image of the whole monitoring area when damages locate in Subarea: (a) 0; (b) 1, 4, and 5; (c) 0, 3, 6, and 7; and (d) 0, 2, 6, 7, and 8.

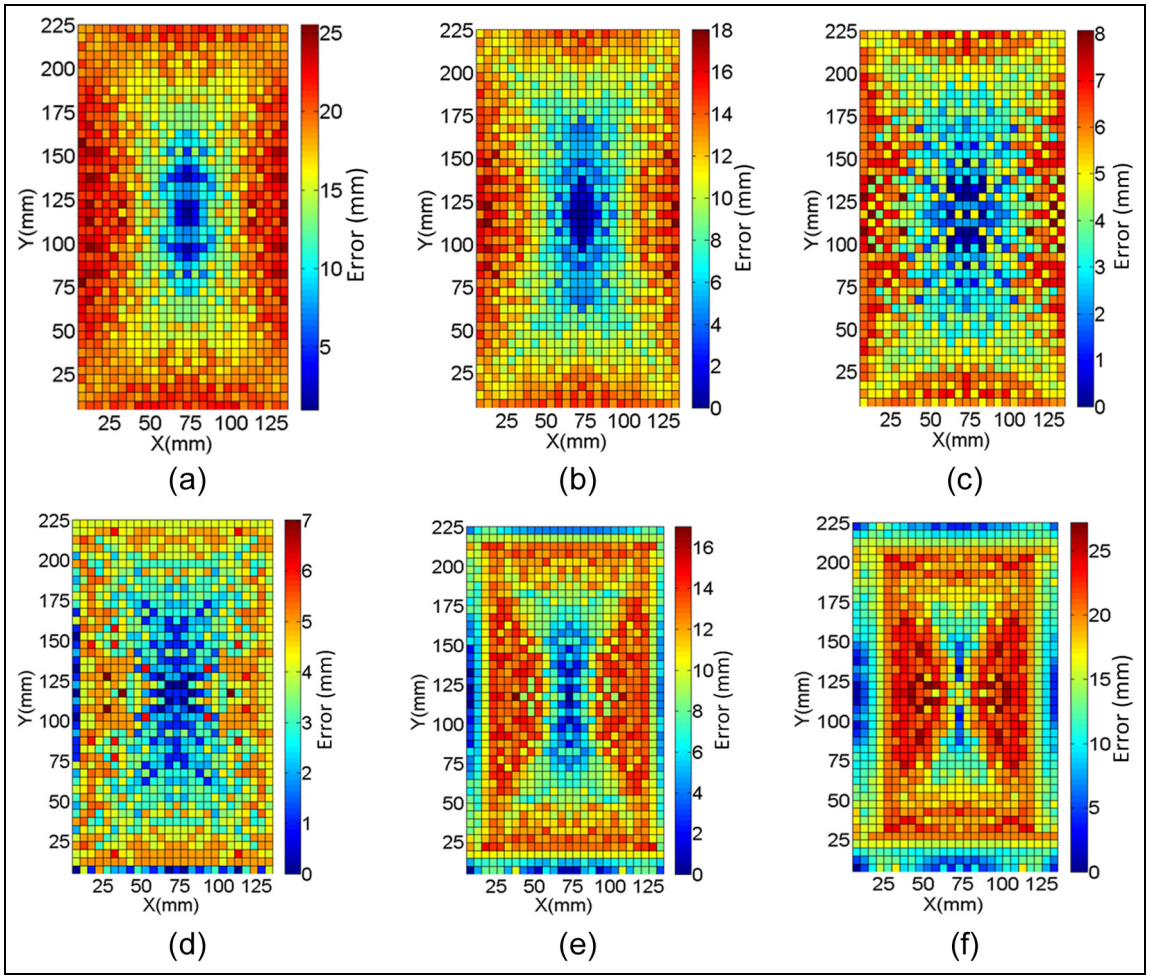

Figure 12. Localization error distribution for a (a) −8%, (b) −5%, (c) −2%, (d) + 2%, (e) + 5%, and (f) + 8% velocity deviation.

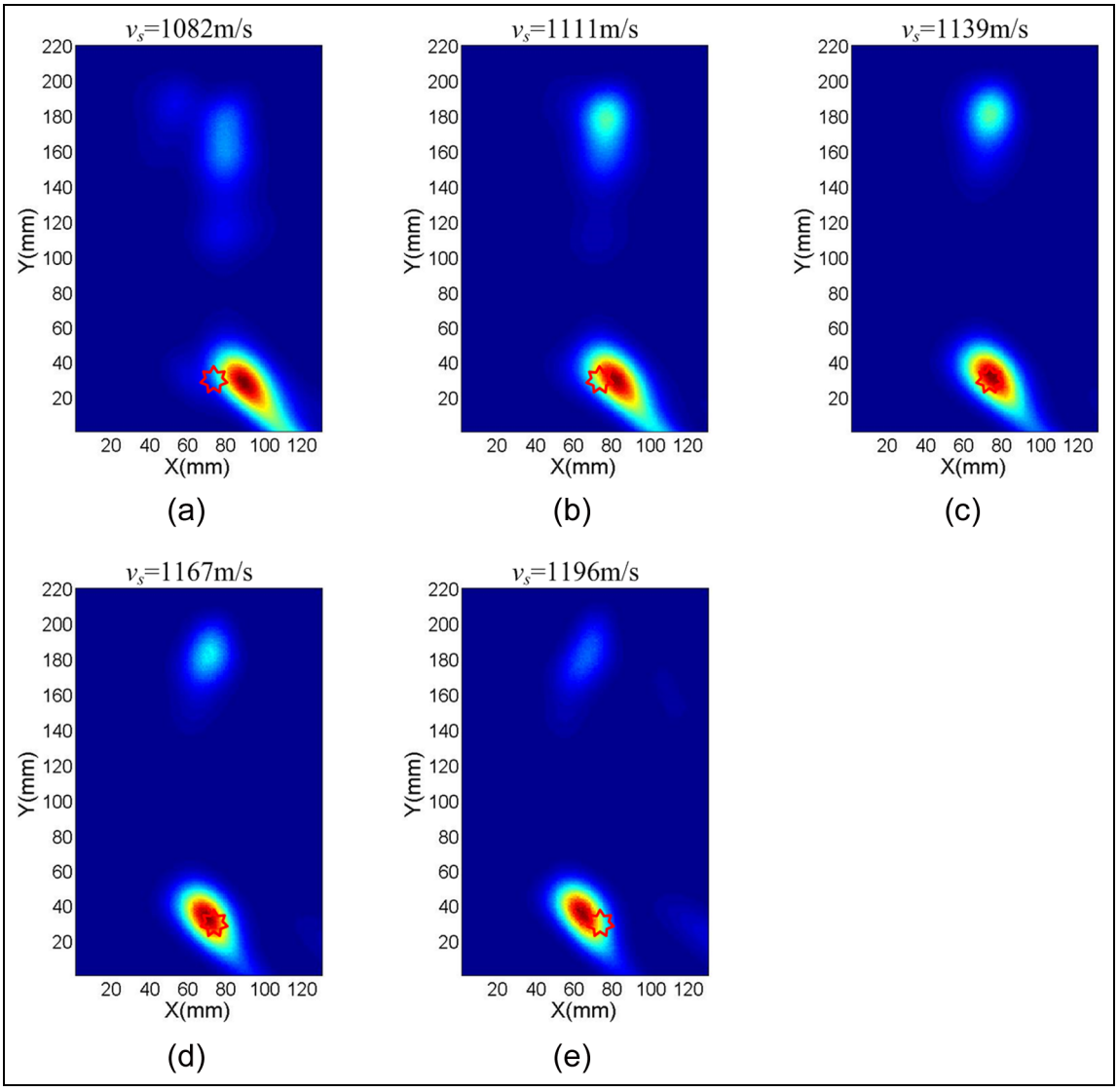

Figure 13. Damage images of Subarea0 when using different preset velocities: (a) −5%, (b) −2.5%, (c) 0%, (d) +2.5%, and (e) +5%; deviation from the actual velocity.

three directions is within the range of ±5%. When there are ±2.5%, 0%, ±5% deviation in the preset group velocity, damage imaging process is carried out in these situations to analyze the corresponding localization errors. As shown in Figure 13(c), the localization accuracy is fairly excellent when choosing the average value of the measured velocities in the three directions. When the deviation is getting larger, the localization accuracy becomes poorer as is predicted in the former discussion. However, within the velocity deviation range from −5% to +5%, the localization error is less than 20 mm. In fact, taking the size of damage into consideration, the calculated damage zones in all the situations overlap with the actual damage. As a result, the system with the damage imaging algorithm has the satisfactory robustness to the preset velocity deviation. In addition, it is proved that this velocity-choice approach for the system is both reasonable and effective.

Boundary processing

When damage locates on the boundary of adjacent subareas, the damage imaging procedure is performed in both the subareas. Figure 14(a) illustrates the damage image of the situation that the multi-damage locates on the boundary of the subareas. Damage information of Subarea3 and Subarea7, Subarea1, and Subarea5 will be redundant in the damage image. After boundary processing, the damage information of the subarea where the *DIA* is relatively small is wiped out and the

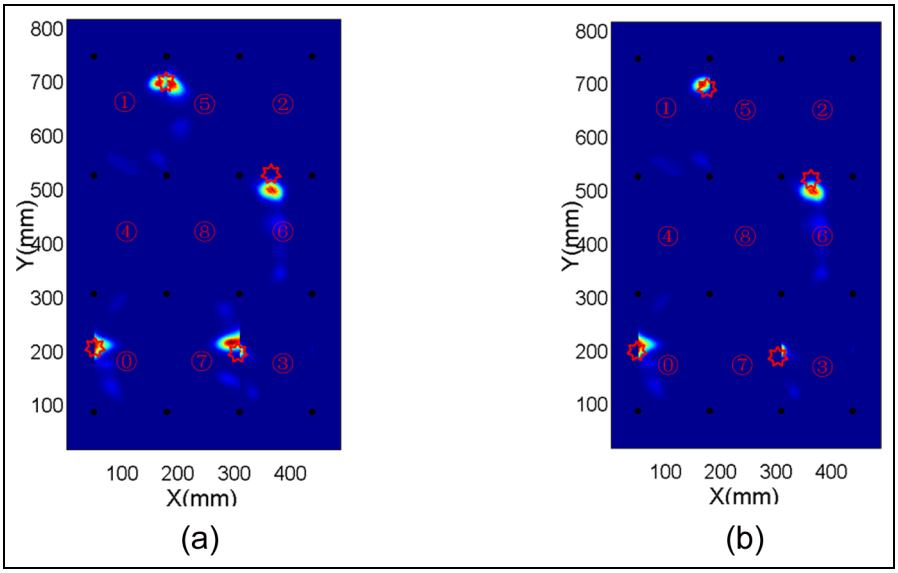

Figure 14. (a) Damage image when damages locate on the boundary of the subareas and (b) damage image after the boundary processing procedure.

resulting damage image is shown in Figure 14(b). The problem about the redundant damage information is appropriately solved and the multi-damage in the damage image is clearly presented.

Conclusion

As an extension of the delay-and-sum method, a multi-damage localization method for complex structures has been proposed. The method was presented in detail and validated with experimental results on a large-scale aircraft panel. The localization accuracy of the delay-and-sum method was significantly improved by the proposed valid data extraction strategy. The multi-damage detection method and boundary processing make the method more adaptive for large structures with multiple damages. In addition, the comprehensive localization accuracy evaluation process quantitatively characterized the relationship between the localization error and the preset velocity.

It is worth mentioning that the proposed method is universally designed for all kinds of transducer network and large complex structures. The multi-damage detection process can serve as a worthwhile experience as it poses the idea that both the geometric property of the structure and propagation characteristics of Lamb waves can be fully exploited for the design of SHM methodology. In addition, the qualities of the valid data extraction strategy and the boundary processing method demonstrate high potential for practical engineering applications. Furthermore, conclusions drawn from the localization accuracy evaluation process can be the guiding tools to help SHM designers to better transplant the method in their applications.

Declaration of Conflicting Interests

The author(s) declared no potential conflicts of interest with respect to the research, authorship, and/or publication of this article.

Funding

The author(s) disclosed receipt of the following financial support for the research, authorship, and/or publication of this article: This work was supported by National High Technology Research and Development Program of China (863 Program) (grant number 2013AA041105), Fundamental Research Funds for the Central Universities (Nos NE2015101 & NE2015001), Research Fund of State Key Laboratory of Mechanics and Control of Mechanical Structures (No. 0515Y02), the "333" project of jiangsu province (No. BRA2015310) and a Project Funded by the Priority Academic Program Development of Jiangsu Higher Education Institutions.

References

1. Giurgiutiu V. *Structural health monitoring with piezoelectric wafer active sensors*. New York: Academic Press, 2014.
2. Staszewski WJ, Boller C and Tomlinson G. *Health monitoring of aerospace structures: smart sensor technologies and signal processing*. Chichester: John Wiley & Sons, 2004.
3. Ostachowicz W and Güemes A. *New trends in structural health monitoring*. Berlin: Springer, 2013.
4. Cawley P and Alleyne D. The use of Lamb waves for the long range inspection of large structures. *Ultrasonics* 1996; 34: 287–290.

5. Su Z and Ye L. *Identification of damage using Lamb waves: from fundamentals to applications*. Berlin: Springer, 2009.
6. Dao PB and Staszewski WJ. Lamb wave based structural damage detection using cointegration and fractal signal processing. *Mech Syst Signal Process* 2014; 49: 285–301.
7. Lee BC and Staszewski WJ. Modelling of Lamb waves for damage detection in metallic structures: part I. Wave propagation. *Smart Mater Struct* 2003; 12: 804–814.
8. Lee BC and Staszewski WJ. Modelling of Lamb waves for damage detection in metallic structures: part II. Wave interactions with damage. *Smart Mater Struct* 2003; 12: 815–824.
9. Liu Y, Chillara VK and Lissenden CJ. On selection of primary modes for generation of strong internally resonant second harmonics in plate. *J Sound Vib* 2013; 332: 4517–4528.
10. Hong M, Su ZQ, Wang Q, et al. Modelling nonlinearities of ultrasonic waves for fatigue damage characterization: theory, simulation, and experimental validation. *Ultrasonics* 2014; 54: 770–778.
11. Wagle S and Kato H. Ultrasonic detection of fretting fatigue damage at bolt joints of aluminum alloy plates. *Int J Fatigue* 2009; 31: 1378–1385.
12. Dixon S, Burrows SE, Dutton B, et al. Detection of cracks in metal sheets using pulsed laser generated ultrasound and EMAT detection. *Ultrasonics* 2011; 51: 7–16.
13. Hongjoon K, Kyungyoung J, Minjea S, et al. Application of the laser generated focused-Lamb wave for non-contact imaging of defects in plate. *Ultrasonics* 2006; 44: 1265–1268.
14. Wandowski T, Malinowski P and Ostachowicz W. Diagnostics using different configurations of sensing networks. In: *Proceedings of the 9th international conference on damage assessment of structures*, Oxford, 11–13 July 2011.
15. Giurgiutiu V. Tuned Lamb wave excitation and detection with piezoelectric wafer active sensors for structural health monitoring. *J Intell Mater Syst Struct* 2005; 16: 291–305.
16. Malinowski P, Wandowski T and Ostachowicz W. Guided waves for aircraft panel monitoring. *Key Eng Mat* 2013; 558: 107–115.
17. Su ZQ, Ye L and Lu Y. Guided Lamb waves for identification of damage in composite structures: a review. *J Sound Vib* 2006; 295: 753–780.
18. Yan F, Royer RL and Rose JL. Ultrasonic guided wave imaging techniques in structural health monitoring. *J Intell Mater Syst Strut* 2010; 21: 377–384.
19. Malinowski P, Wandowski T, Trendafilova I, et al. A phased array-based method for damage detection and localization in thin plates. *Struct Health Monit* 2009; 8: 5–15.
20. Zhao X, Royer R, Owens E, et al. Ultrasonic Lamb wave tomography in structural health monitoring. *Smart Mater Struct* 2011; 20: 105002–105011.
21. Zhao X, Gao H, Zhang G, et al. Active health monitoring of an aircraft wing with embedded piezoelectric sensor/actuator network: I. Defect detection, localization and growth monitoring. *Smart Mater Struct* 2007; 16: 1208–1218.
22. Wu ZJ, Liu KH, Wang YS, et al. Validation and evaluation of damage identification using probability-based diagnostic imaging on a stiffened composite panel. *J Intell Mater Syst Strut*. Epub ahead of print 9 September 2014. DOI: 10.1177/1045389X14549873.
23. Wang CH, Rose JT and Chang FK. A synthetic time-reversal imaging method for structural health monitoring. *Smart Mater Struct* 2004; 13: 415–423.
24. Ng CT and Veidt M. A Lamb-wave-based technique for damage detection in composite laminates. *Smart Mater Struct* 2009; 18: 1–12.
25. Sharif-Khodaei Z and Aliabadi MH. Assessment of delay-and-sum algorithms for damage detection in aluminium and composite plates. *Smart Mater Struct* 2014; 23: 075007.
26. Wang D, Ye L, Su Z, et al. Quantitative identification of multiple damage in laminated composite beams using A0 Lamb mode. *J Compos Mater* 2011; 45: 2061–2069.
27. Qiu L, Liu ML, Qing XL, et al. A quantitative multi-damage monitoring method for large-scale complex composite. *Struct Health Monit* 2013; 12: 183–196.
28. Lin J and Qu LS. Feature extraction based on Morlet wavelet and its application for mechanical fault diagnosis. *J Sound Vib* 2000; 234: 135–148.
29. Hu N, Cai Y, Zhu G, et al. Characterization of damage size in metallic plates using Lamb wave. *Struct Health Monit* 2012; 11: 125–137.
30. Hu N, Shimomukai T, Yan C, et al. Identification of delamination position in cross-ply laminated composite beams using S_0 Lamb mode. *Compos Sci Technol* 2008; 68: 1548–1554.